Droplet size dependency and spatial heterogeneity of lipid oxidation in whey protein isolate-stabilized emulsions

Suyeon Yang[a,1], Sten ten Klooster[b,1], Khoa A. Nguyen[c], Marie Hennebelle[c], Claire Berton-Carabin[b,d], Karin Schroën[b], John P.M. van Duynhoven[a,e,*], Johannes Hohlbein[a,f,*]

[a] Laboratory of Biophysics, Wageningen University & Research, Stippeneng 4, 6708 WE Wageningen, the Netherlands

[b] Laboratory of Food Process Engineering, Wageningen University & Research, 6708 WG, Wageningen, The Netherlands

[c] Laboratory of Food Chemistry, Wageningen University & Research, 6708 WG, Wageningen, The Netherlands

[d] INRAE, UR BIA, 44300 Nantes, France

[e] Unilever Global Foods Innovation Centre, Plantage 14, 6708 WJ Wageningen, the Netherlands

[f] Microspectroscopy Research Facility, Wageningen University & Research, Stippeneng 4, 6708 WE Wageningen, the Netherlands

[1] These authors contributed equally.

[*] Corresponding authors: john.vanduynhoven@wur.nl (John P.M. van Duynhoven), johannes.hohlbein@wur.nl (Johannes Hohlbein).

Abstract

Spatiotemporal assessment of lipid and protein oxidation is key for understanding quality deterioration in emulsified food products containing polyunsaturated fatty acids. In this work, we first mechanistically validated the use of the lipid oxidation-sensitive fluorophore BODIPY 665/676 as a semi-quantitative marker for local peroxyl radical formation. Next, we assessed the impact of microfluidic and colloid mill emulsification on local protein and lipid oxidation kinetics in whey protein isolate (WPI)-stabilized emulsions. For that purpose, we also used BODIPY 581/591 C11 and CAMPO-AFDye 647 as colocalisation markers for lipid and protein oxidation. The polydisperse emulsions showed an inverse relation between droplet size and lipid oxidation rate. Further, we observed less protein and lipid oxidation occurring in similar sized droplets in monodisperse emulsions. This observation was linked to more heterogeneous protein packing at the droplet surface during colloid mill emulsification, resulting in larger inter-droplet heterogeneity in both protein and lipid oxidation. Our findings indicate the critical roles of emulsification methods and droplet sizes in understanding and managing lipid oxidation.

Keywords: monodisperse, lipid oxidation, protein oxidation, interfacial heterogeneity, modelling kinetic reactions

1 Introduction

Lipid oxidation is a major factor contributing to the deterioration of the sensorial quality of food products containing oil rich in unsaturated fatty acids.[1] In many of these products, oil is dispersed as droplets in a continuous aqueous phase,[2] such as sauces, dressings, and infant milk. In these oil-in-water (O/W) emulsions, lipid oxidation is enhanced by the large interfacial area at which pro-oxidants present in the continuous aqueous phase are close to the lipids.[1,3] Lipid oxidation can be mitigated by utilizing synthetic antioxidants, packaging the products in inert atmospheres, and storing products at low temperatures.[3] Although these measures are very effective, the food industry faces pressure to develop alternative solutions. The main drivers are the need for a more sustainable supply chain and the clean labeling trend urging manufacturers to refrain from using synthetic antioxidants.[3]

Furthermore, benefits associated with cardiovascular health-promoting products with high levels of polyunsaturated fatty acids (PUFAs) such as omega-3 fatty acids[4,5] are of increasing interest. However, PUFAs are particularly susceptible to lipid oxidation.[6,7] All these aspects have rekindled the research interest in lipid oxidation and its prevention in O/W emulsions. Most of our current knowledge has been obtained using one-dimensional methods[8] that measure markers of lipid oxidation in an extracted oil phase.[9,10] However, none of these methods capture the complexity of lipid oxidation kinetics occurring at the surface or within colloidal structures.[11] The complexity of lipid oxidation in O/W emulsions from the perspective of location and time has urged the field to shift from one-dimensional to spatiotemporally resolved research approaches.[12]

To resolve the spatiotemporal aspects of lipid oxidation in food emulsions, confocal laser scanning microscopy (CLSM) is increasingly being deployed.[13–16] Using CLSM and fluorescent BODIPY dyes[17] enables the monitoring and localization of lipid oxidation as these BODIPY dyes undergo changes in absorption and emission spectra upon oxidation. For example, a recent publication using BODIPY 665/676 showed that oxidation in medium chain triglyceride (saturated fatty acids) emulsion droplets occurred faster when co-oxidizing unsaturated oil droplets were present.[14] This may indicate that lipid oxidation can spread from oxidizing droplets to non-oxidized ones or that oxidizing droplets influence each other. A different study using the same fluorophore showed, however, that when lipid oxidation is selectively initiated in a single droplet, the oxidation does not spread rapidly to neighboring droplets.[18] Recently, we used BODIPY 665/676 to show that the formulation of the emulsions determined the effect of droplet size on lipid oxidation in an O/W emulsion with a high oil concentration, such as mayonnaise.[16] In that study, we combined information from monitoring local changes in BODIPY 665/676 fluorescence with local protein autofluorescence at the single-droplet level. Despite much ambiguity in the literature on the role of

droplet size dispersion and heterogeneity of lipid oxidation, no systematic spatiotemporally-resolved investigation has yet been performed.[15,19–21]

Here we first mechanistically validate the use of BODIPY 665/676 to monitor local lipid oxidation in protein-stabilized emulsions. Then, using a quantitative kinetic reaction model, we assess the scope of using BODIPY 665/676 as a peroxyl radical monitor. Next, we focus on the spatiotemporal heterogeneity of lipid oxidation in mono- and polydisperse WPI-stabilized emulsions, respectively, prepared by a conventional method (colloid mill) and by microfluidic emulsification. By using the fluorescent spintrap CAMPO-AFDye 647, lipid and protein oxidation could be co-localized.

2 Materials and methods

2.1 Materials

Soybean oil was kindly supplied by Unilever (Wageningen, the Netherlands). Sodium phosphate dibasic heptahydrate (MW: 268.07 g/mol), sodium phosphate monobasic monohydrate (MW: 137.99 g/mol), and phosphoric acid (85.0-88.0%) were purchased from Sigma-Aldrich (Zwijndrecht, the Netherlands) to prepare a 10 mM phosphate buffer (pH 3.0). n-Hexane and 2-propanol were obtained from Actu-All Chemicals (Oss, the Netherlands). Deuterated chloroform and dimethylsulfoxide ($CDCl_3$ and DMSO-d6) were purchased from Euriso-top (Saint-Aubin, France). Tween 20 was purchased from Sigma Aldrich (Zwijndrecht, the Netherlands). WPI, purity 97.0–98.4% (BiPro®, Davisco, Switzerland) was used as received. For cleaning the microfluidic chips, we used ethanol, purity of 96% v/v (VWR International B.V., Amsterdam, the Netherlands) and piranha solution, which represents a 3:1 v/v ratio of sulphuric acid, a purity of 96% (Sigma-Aldrich, Zwijndrecht, the Netherlands) and 35 wt.% hydrogen peroxide (Sigma-Aldrich, Zwijndrecht, the Netherlands). The assay reagent for measuring the triacylglycerol (TAG) content and a standard containing TAGs (Triglycerides liquicolor mono kit) were purchased from HUMAN (HUMAN Gesellschaft für Biochemica und Diagnostica mbH, Wiesbaden, Germany). The assay reagent comprised 50 mmol/L PIPES buffer (pH 7.5), 5 mmol/L 4-chlorophenol, 0.25 mmol/L 4-aminoantipyrine, 4.5 mmol/L magnesium ions, 2 mmol/L ATP, 1.3 U/mL lipases, 0.5 U/mL peroxidase, 0.4 U/mL glycerol kinase and 1.5 U/mL glycerol-3-phosphate oxidase. The lipophilic and oxidation-sensitive dyes BODIPY 665/676 and BODIPY 581/591 C11 were purchased from Thermo Fischer (Waltham, MA, USA). CAMPO-AFDye 647 was synthesized by SyMO-Chem B.V. (Eindhoven, the Netherlands). 2,2'-Azobis (2-amidinopropane) dihydrochloride (AAPH) and sodium azide were purchased from Sigma Aldrich (Zwijndrecht, the Netherlands).

Ultrapure water (18.2 MΩ) was used for all experiments and prepared using a Milli-Q system (Millipore Corporation, Billerica, MA, USA).

2.2 Preparation and incubation of emulsions

2.2.1 Preparation of oil and the continuous water phase

Soybean oil was stripped with alumina powder (MP112 EcoChromet ALUMINA N, Activity: Super I, Biomedicals) to remove impurities and endogenous antioxidants such as tocopherols[22]. For both emulsification methods (i.e., colloid mill and microfluidics, see below), the oil was filtered using a 0.22-µm filter (Minisart High-Flow, Sartorius Stedim Biotech GmbH, Goettingen, Germany) to remove any small particles that can cause clogging of the microfluidic channels. To prepare the continuous phase, either Tween 20 or WPI was dissolved in a 10 mM phosphate buffer (pH 3.0) with a concentration of 2.35 wt.%. Next, the mixture was stirred for 2 hrs (WPI) or 30 min (Tween 20). For the lipid oxidation experiments, BODIPY 665/676 was added to the stripped soybean oil (final concentration of 1 or 50 µM) before making emulsions.

2.2.2 Colloid mill emulsification

A coarse emulsion was made by adding 15 wt.% of the stripped soybean oil (with or without BODIPY 665/676) to the continuous aqueous phase, and high-speed stirring was applied at 11,000 rpm for 1 min with a rotor-stator homogenizer (Ultra-turrax IKA T18 basic, Germany). A fine emulsion was prepared by passing the coarse emulsion through a lab-scale colloid mill with a gap width of 0.32 mm (IKA Magic Lab, Staufen, Germany), operating for 1 min at 26,000 rpm. During operation, the colloid mill was cooled with water at 4 °C.

2.2.3 Microfluidic emulsification

To produce monodisperse emulsions, the microfluidic emulsification chip called UPE$_{10\times1}$ (Upscaled Partitioned EDGE [Edge-based droplet generation]) was used (**Figure S2**).[23] These chips were designed in our lab and produced in glass by deep reactive ion etching (Micronit Microfluidics, Enschede, The Netherlands). A chip with 8,064 droplet formation units (DFUs) of 10 × 1 µm (width × height) each was used. More details about the fabrication, operation, and droplet formation were described in the literature.[23]

2.2.4 Emulsion handling and incubation

Sodium azide (0.05 wt. %) was added to the emulsions to prevent accidental growth of bacteria. For lipid-protein co-oxidation measurements, BODIPY 581/591 C11 was added to the emulsions prior to incubation, and CAMPO-

AFDye 647 (see **Figure S1** for the chemical structure) was added after incubation, before the measurements. The concentrations of BODIPY 581/591 C11 and CAMPO-AFDye 647 in the emulsions were 1 µM.

To initiate lipid oxidation, 5 mM of 2,2'-azobis (2-amidinopropane) dihydrochloride (AAPH) was added to the emulsions. 0.2 mL emulsion sample was added to 1.5 mL microcentrifuge tubes. The tubes were rotated horizontally at 2 rpm in a dark oven at 25 °C for up to 10 days. At sampling time points, two tubes per independently prepared emulsion were taken and either used directly for further measurements (imaging with CLSM) or stored under inert gas at -80 °C for at least 48 hrs for lipid extraction and, subsequently, quantification of lipid oxidation products.

2.3 Determination of lipid oxidation in bulk

2.3.1 Initial O_2 concentration

The initial O_2 amount of ~ 450 mmol/kg oil was calculated using a headspace volume of 1.55 mL with 20.9 % O_2 partial pressure; 46.8 mg/kg O_2 concentration in the oil,[24] and 8.1 mg/kg O_2 concentration in the continuous aqueous phase.[25]

2.3.2 Oil extraction

The extraction of lipids and of lipid oxidation products was performed by adding 1 mL hexane-isopropanol (3:2 v/v) to ~ 1.5 mL emulsion and vortexing thoroughly, as described previously.[26,27] The mixture was centrifuged at 4,000x*g* for 20 min, and the upper layer, containing hexane and extracted lipids, was carefully separated from the bottom layer. Hexane was evaporated under a stream of nitrogen at 25 °C until constant weight, and the remaining oil was treated with a nitrogen blanket and frozen at -80 °C for at least 48 hrs until further measurements were performed.[28]

2.3.3 Lipid oxidation measurements by quantitative ^{1}H NMR

Hydroperoxides (primary oxidation products), aldehydes (secondary oxidation products) and triacylglycerols (as a reference for the total amount of oil) were simultaneously quantified using ^{1}H NMR, with an Advance III 600 MHz spectrometer, equipped with a 5-mm cryo-probe at 295 K, following the method described earlier.[29] In brief, 580 µL of a mixture of $CDCl_3$/DMSO-d6 (5:1 v/v) were added to ~ 20 µL extracted oil (as described in the previous section) and transferred to 5-mm NMR tubes (Bruker, Billerica, Massachusetts, USA). From the recorded single pulse experiment, the glycerol backbone peaks at δ 4.4 pm were used to quantify the amount of triacylglycerols. With a band selective pulse, the region between δ 13.0 and 8.0 ppm was selectively excited for the quantification

of hydroperoxides and aldehydes, following Merkx et al..[29] The hydroperoxide signals resonate between δ 11.3 and 10.6 ppm, and the aldehydes resonate between δ 9.8 and 9.4 ppm. The calculations, including a factor that accounts for intensity loss during the selective pulse, are described elsewhere.[29] The data were processed with the Bruker TopSpin 4.0.6 software.

2.4 Monitoring local lipid and protein oxidation

2.4.1 Confocal laser scanning microscopy (CLSM)

The emulsion samples were centrifuged for 5 min at 2,000 rpm, and the cream layer was taken. This procedure was used to prevent the droplets from moving during the CLSM measurement. A silicon gasket was fixed on the cleaned glass, and 2 µL of the cream phase was dripped into a well of a silicon gasket (CultureWell™, GRACEBIO-LABS). The well was then sealed with a glass plate to prevent the evaporation of water from the samples. Fluorescence images were recorded on a confocal laser scanning microscope (CLSM, Leica SP8) equipped with a 63 x NA = 1.2 water immersion objective (HC PLAPO CS2, Leica) and a white-light laser with user-selectable excitation wavelengths. The scanning format was 512 × 512 pixels (i.e., 62 µm × 62 µm), and the line-scanning speed was set to 100 Hz. For lipid oxidation measurements with BODIPY 665/676, the excitation wavelengths were set to 561 and 640 nm to detect oxidized and non-oxidized lipids, respectively. Detection ranges were set from 580 to 660 nm and 660 to 750 nm, respectively. For protein oxidation measurements with CAMPO-AFDye 647, the samples were excited at 640 nm with a detection range between 660 and 750 nm. BODIPY 581/591 C11 was excited at 561 and 488 nm to detect non-oxidized and oxidized BODIPY, respectively. The emission ranges were set from 580 to 660 nm and 500 to 560 nm, respectively.

2.4.2 Local lipid oxidation

CLSM imaging data were analyzed using StarDist[30] and MATLAB R2021b software (Math works, Natick, MA, USA). First, the raw image data from non-oxidized (ex 640 nm for BODIPY 665/676 and ex 561 nm for BODIPY 581/591 C11) and oxidized (ex 561 nm for BODIPY 665/676 and ex 488 nm for BODIPY 581/591 C11) channels were summed and used for the segmentation of oil droplets in 2D StarDist. In the segmentation steps, the versatile (fluorescence nuclei) model was used for the neural network prediction. We set the percentile low and high values to 1 and 99.8, respectively. The probability/score threshold was set to 0.5, and the overlap threshold was 0.4. After the segmentation steps, the masks were applied to the raw image data for the analysis of the fluorescence intensity changes using MATLAB. The average intensity and radii were determined for each droplet by summing up the total number of pixels for each segmented region and assuming a circle for each region. Then the radius was

calculated from the square root of the area divided by π with 1 pixel corresponding to an area of 0.12 by 0.12 µm. For the normalized data set, the averaged intensities of red fluorescence in each droplet were divided by the total average red fluorescence intensity in the fresh sample (**Figure S3**). At least 2000 oil droplets with diameters between 1 and 6 µm were used for the analyses at each time point.

2.4.3 Local protein oxidation

The mask from oil droplet segmentation was applied to the maps of trapped protein radicals measured via accumulation of the spin trap CAMPO-AFDye 647 (ex 640 nm). Next, the applied images were filtered to visualize only the accumulation of the CAMPO-AFDye 647 at the droplet interface. Filtered images were obtained by applying the segmentation mask from the oil droplets on the raw data. Then, to remove the background intensity from within the oil droplets, only the pixels with intensity counts exceeding 30% of the maximum fluorescence intensity from all segmented droplets were considered for further calculation. With these segmented images, the level of trapped protein radicals per droplet was determined by first summing up all the intensities per droplet and dividing it by the circumference of the droplet using the radius which we obtained from the area in pixels after segmentation.

2.5 Droplet size measurements

2.5.1 Static light scattering (SLS)

The oil droplet size of the whole emulsions was measured by static light scattering (SLS) (Malvern Mastersizer 3000, Malvern Instruments Ltd., Malvern, Worcestershire, UK), using a refractive index of 1.465 for the dispersed phase and 1.33 for the dispersant (water); and an absorption index of 0.01.

2.5.2 Dynamic light scattering (DLS)

The continuous aqueous phase and the smallest oil droplets were separated from the larger oil droplets by centrifuging 2 mL of emulsion at 20,000 *g* for 42 min in a 2-mL microcentrifuge tube and collecting ~ 0.3 mL of the subnatant from the bottom of the tube as previously reported.[31] The size of the colloidal structures present in this subnatant was measured by dynamic light scattering (DLS) (Zetasizer Nano ZS, Malvern Instruments Ltd., Malvern, Worcestershire, UK). The refractive index (unitless) was 1.47 for the dispersed phase, and the absorbance was 0.01.

2.5.3 Oil content

The amount of lipids corresponding to tiny droplets was quantified using a colorimetric method for measuring the triacylglycerol content (Triglycerides Liquicolor Mono kit, HUMAN).[32,33] In brief, the subnatant samples, obtained as described in the section above, were diluted to a range of 0.4-4 g/L, and about 20 µL of the sample was weighed into a 2-mL microcentrifuge tube. Next, 1 mL of assay reagent was added, and the samples were subsequently incubated in a heating block at 800 rpm for 20 min at 20 °C. The absorbance was measured at a wavelength of 500 nm, and the concentration was calculated using a calibration curve (0.4-4 g triglycerides/L).

2.5.4 Combined droplet size distribution

For visualization purposes, the droplet size distributions obtained by DLS and SLS were superimposed on the same graph. The relative intensities from the DLS measurements were adjusted based on the actual oil contents in the subnatant. The relative intensities from the SLS measurements were adjusted based on the assumption that its oil content was one minus the oil content in the subnatant. Finally, the surface-volume mean diameter (D_{32}) was calculated as:

$$D_{32} = \frac{\sum_i n_i d_i^3}{\sum_i n_i d_i^2,} \quad (1)$$

where n_i is the number of droplets (unit-less) of a diameter d_i (in μm).

2.5.5 Confocal laser scanning microscopy (CLSM)

The droplet sizes of monodisperse emulsions were measured by CLSM. The same segmentation steps (section 2.4.2) were applied to the raw images. The number of pixels was counted per droplet, and the radius was calculated based on the sum of pixels (**Figure S3**).

2.6 Experimental design

For each experimental measurement, at least two emulsion samples were independently prepared, except for the measurements with emulsions containing 50 µM of BODIPY 665/676, for which only one emulsion sample was prepared. Additionally, droplet size and lipid oxidation measurements were performed on two independently incubated samples from the same emulsion for each sampling time point.

2.7 Quantitative kinetic model

2.7.1 Lipid oxidation reactions in the kinetic model

A kinetic model was constructed from our datasets to describe lipid oxidation reactions (in **Table 1**) by first (R.1 and R.4) and second order reactions.[34] The reactivity of AAPH and BODIPY in the system was accounted for by reactions R.8 and R.9 (**Table 1**) in the kinetic model.[34]

To estimate the impact of changes in D_{32} on the formation of lipid oxidation products, we varied D_{32} with deviations of σ. The concentration over time of the compounds with D_{32} was denoted as $[C]$. Then, with $D_{32} \pm \sigma$, the varied concentration denoted as $[\tilde{C}]$ can be calculated as (see **Supplementary materials**).

$$[\tilde{C}] = \frac{D_{32}}{D_{32} \pm \sigma} \times [C]. \quad (2)$$

The final model described by equations S1 to S11 relates the concentrations of O_2 and AAPH at the oil-water interface to droplet sizes using their partition coefficients and D_{32}.

2.7.2 Estimation of kinetic constants and initial radical concentrations

The final model required estimating 13 parameters: k_1 to k_7 (R.1 – R.7, **Table 1**), k_{AAPH} and k_{BODIPY} (R.8 and R.9, **Table 1**), and initial concentration of L*, LOO*, LO*, and OH*. The model equations (**Table S1**) substituted by the estimated values (**Table S2**) described and explained our experimental data well. We do not recommend to use these estimates to generate model predictions for other emulsion samples. Our current study does not focus on model predictions.

These parameters were estimated using a global multi-response optimization method[35], i.e., by fitting hydroperoxide and aldehyde profiles simultaneously, using MATLAB 2021b software (Mathworks, Natick, MA, USA) [36]. The optimization procedure was applied to fit experimental datasets with 1 µM BODIPY 665/676. Based on the literature, k_3 (R.3 in **Table 1**) was found to be approximately two times lower than k_{BODIPY} (R.9 in **Table 1**),[37] thus, we fixed k_3 as $0.5 \times k_{BODIPY}$. Typically, the starting values of all parameters required for the optimization were obtained from the literature (**Table S2**).[38,39] Then, for every set of initial starting values, the *'lsqnonlin'* algorithm simultaneously determined their estimated values by minimizing the sum of the squared residuals between the experimental (X_{exp}) and numerical (X_{num}) datasets.

In our dataset, measured by ^{1}H-NMR, the concentration of hydroperoxides varied between 0 and 400 mmol/kg oil, while the concentration of aldehydes varied between 0 and 6 mmol/kg oil. To be equally weighted in the

optimisation procedure, the datasets ($\tilde{X}$) were thus normalized to be the same range of 0 and 1, following **Equation 3** before calculating the sum of squared errors (**Equation 4**). As each set of starting values returned different estimated values, the optimal estimated values were selected based on the least estimate of errors (**Equation 4**).

$$\tilde{X}_i = \frac{X_i - min(X_{exp})}{max(X_{exp}) - min(X_{exp})}, \quad (3)$$

where subscript i denotes either a numerical or experimental curves, and exp represents experimental kinetic curves.

$$\left\|\tilde{X}_{\text{exp}} - \tilde{X}_{\text{num}}\right\|_2^2 = \sum_{i=1}^{n_t} \left(\tilde{X}(t_i)_{\text{exp}} - \tilde{X}(t_i)_{\text{num}}\right)^2, \quad (4)$$

where $t, i,$ and n_t indicate storage time, index of time points, and the total number of time points, respectively. After fitting the numerical and experimental datasets, the precision of the estimated values was evaluated using Monte Carlo simulations with 200 iterations to calculate the standard deviations[40]

$$X_{\text{noise,exp}} = X_{\text{exp}} + \sigma r_1 r_2, \quad (5)$$

where X_{noise}, and X_{exp} are the noised and original experimental data, respectively. σ is the experimental standard deviation estimated for each experimental data, and r_1 and r_2 are random values varying from 0 to 1.

2.7.3 Simulation of the impact of BODIPY 665/676 and droplet size on lipid oxidation

Using the estimates of 13 parameters (**Table S1**), the formation of lipid oxidation products was simulated over time with BODIPY 665/676 concentrations of 0, 1 and 50 µM and with a fixed D_{32} value. Then the simulated data were compared with the experimental datasets measured by ^{1}H-NMR. To illustrate the impact of droplet sizes on lipid oxidation products, model simulations were conducted using D_{32} + 0.2 µm and D_{32} - 0.2 µm, while keeping the initial concentration (1 µM) of BODIPY fixed. Furthermore, we simulated the concentration of native BODIPY 665/676 over time and compared it with the decrease in the experimentally obtained and normalized red fluorescence intensities. The integral of peroxyl radicals (LOO*) over time was also calculated based on the reaction mechanisms.

3 Results and discussion

3.1 Microstructural characterization of WPI-stabilized emulsions

Poly- and monodisperse emulsions were prepared with a lab-scale colloid mill or by microfluidic emulsification. The droplet size distribution of colloid mill-made emulsions was obtained using DLS and SLS, and the droplet

size distribution of microfluidic-made emulsions was obtained using CLSM. The surface volume mean diameter (Sauter mean diameter, D_{32}) of the colloid mill-made emulsion, stabilized by WPI, obtained from SLS and DLS was 1.4 µm (**Figure 1**). By centrifugation of the colloid mill emulsions, a subnatant was obtained, which contained tiny droplets (< 200 nm diameter).[41] Such tiny droplets were also observed in previous work by electron microscopy.[31] The size distribution of these tiny droplets, as determined by DLS, and their volume fraction is shown in **Figure 1**. The WPI-stabilized emulsion made with microfluidics showed a D_{32} of 4.5 µm (obtained from CLSM), which is larger than for the colloid-mill made emulsions, although their size distributions partially overlap.

3.2 Mechanistic validation of BODIPY 665/676 as a quantitative marker for local lipid oxidation

BODIPY 665/676 has been previously used as a marker to localize lipid oxidation in food emulsions.[13–16] Oxidation of BODIPY 665/676 can be detected by a shift of fluorescence emission from the red to the green spectral region upon reaction with peroxyl radicals.[42,43] This reaction causes the cleavage of the phenylbutadiene moiety and the formation of an acid group, which can occur at several positions (**Figure S4**).[37,44] It has been reported that peroxyl radicals react more rapidly with BODIPY 665/676 (R.9, **Table 1**) than with unsaturated fatty acids (R.3, **Table 1**).[37] However, whether these reactions interact or compete with lipid oxidation is unclear. BODIPY 665/676 may, for example, partially inhibit the formation of hydroperoxides and aldehydes following reactions 3 and 4 (**Table 1**). We therefore carried out a mechanistic validation of using the fluorescence change of BODIPY 665/676 as a quantitative marker for lipid oxidation.

First, we measured the concentrations of hydroperoxides and aldehydes in 2 wt.% WPI-stabilized polydisperse emulsions over ten days with 0, 1 or 50 µM BODIPY 665/676 in the oil phase and using ^{1}H-NMR. These polydisperse emulsions were prepared with separate colloid mill preparations as the different BODIPY 665/676 levels needed to be added to the oil phase before emulsification. The kinetic curves in **Figure 2a & b** show that the emulsion prepared with BODIPY 665/676 oxidized less rapidly than those that did not contain BODIPY 665/676, except for after six days, when the values started to reach a plateau (**Figures 2a & b**). In an independent experiment, however, emulsions with 1 µM BODIPY showed slightly faster oxidation than the emulsions without (0 µM) BODIPY (**Figure S7**).

To assess the influence of adding BODIPY 665/676 on lipid oxidation in a systematic manner, the kinetic model was used to simulate the formation of lipid oxidation products in the presence of BODIPY 665/676. In this model, the kinetic constants and initial radical concentrations were estimated by fitting the numerical kinetic profiles[39] of

hydroperoxides and aldehydes to the experimental datasets with 1 µM BODIPY 665/676. With the estimates (**Table S2**), the concentrations of oxidation products and all other parameters were simulated as used in the experiments.

It was reported earlier that the reaction of BODIPY 665/676 with peroxyl radicals (k_{BODIPY} in R.9, **Table 1**) has a higher kinetic constant than the formation of lipid hydroperoxides (k_3 in R.3, **Table 1**).[37] Our results show, however, that although k_{BODIPY} was two times higher than k_3, the kinetic rate of the reaction between BODIPY 665/676 and peroxyl radicals is 4.5×10^7 times slower than the hydroperoxide formation, which is due to the high initial concentration of lipid substrates (see **Supplementary materials**). This finding explains, why our simulation showed that at the low concentration working range ($\leq$ 50 µM), BODIPY 665/676 does not influence the formation of lipid oxidation products. Using a 10^4 higher concentration of BODIPY 665/676 (500 mM) our simulations showed a higher reaction rate than hydroperoxide formation, resulting in a slower lipid oxidation rate (**Figure S5**). The simulations further showed that the differences in the experimentally obtained kinetic curves between emulsions including 0, 1, or 50 µM of BODIPY 665/676 (**Figures 2a & b**) could not be attributed to the concentration of BODIPY 665/676.

We note that our emulsions were independently prepared, leading to potential variations in droplet size distributions. Hence, we simulated hydroperoxide and aldehyde kinetic curves for an emulsion with surface-volume mean diameter (D_{32}) of 1.2, 1.4, and 1.6 µm (**Figure S6**). The simulations show a clear difference in the kinetic curves for variations in D_{32}, which indicates that the variation in kinetic curves in **Figure 2** can be attributed to minor variations in the distribution of droplet sizes.

Next, to establish a quantitative interpretation of a change in BODIPY 665/676 fluorescence, we used mechanistic simulations and compared the experimental fluorescence data with 1 µM of BODIPY 665/676. BODIPY 665/676 is known to react with LOO*, which makes BODIPY 665/676 an effective lipid oxidation marker. The correlation between BODIPY 665/676 and the concentration of LOO* is, however, still unclear. Direct measurements of LOO* in emulsions are experimentally difficult due to the short lifetime of this radical; therefore, the LOO* concentration was simulated using the kinetic model. The concentration of native BODIPY 665/676 over time was calculated as

$$[\mathrm{BODIPY}(t)] = [\mathrm{BODIPY}(0)] - \int_0^{\mathrm{T}} k_{\mathrm{BODIPY}} \times [\mathrm{LOO}^*(t)] \times [\mathrm{BODIPY}(t)]\mathrm{dt}, \quad (6)$$

where BODIPY 665/676 is used in a working range of 1 - 50 µM. The integral term in **Equation 6** indicates BODIPY 665/676 consumption over time. As a simplified expression, **Equation 6** can be written as

$$[\mathrm{BODIPY}(t)] \approx [\mathrm{BODIPY}(0)] - \int_0^T k'_{\mathrm{BODIPY}} \times [\mathrm{LOO}^*(t)]\,\mathrm{dt}, \quad (7)$$

where [BODIPY(t)] and [LOO*(t)] (in mmol/kg oil) indicate concentrations of BODIPY 665/676 and peroxyl radicals (LOO*) at time t within the range of 0 to storage time T, respectively, and $k'_{\mathrm{BODIPY}} = k_{\mathrm{BODIPY}} \times [\mathrm{BODIPY}(0)]$.

In **Figure 2c**, the decrease in experimental red fluorescence intensity of BODIPY 665/676 upon oxidation was compared with the simulated concentration of the native state of BODIPY 665/676 using the kinetic model. The agreement between experimental and simulation data (from **Equation 6** and 7) indicates that the model can adequately describe the concentration of native BODIPY 665/676. Furthermore, the approximate concentration of LOO* (from **Equation 7**) indicates that a decrease in BODIPY 665/676 fluorescence can be simply interpreted as the integral of [LOO*] over time which cannot be measured experimentally (**Figure 2d**).

3.3 Lipid oxidation in WPI-stabilized mono- and polydisperse emulsions

Emulsion samples containing 2 wt.% of WPI and prepared with either microfluidic emulsification[23] or a lab scale colloid mill were incubated with 5 mM AAPH at 25 °C in the dark. Hydroperoxides (HP) and aldehydes (ALD) were quantified over incubation (**Figures 3a & b**), and the decrease in red fluorescence emission of BODIPY 665/676 was measured with CLSM (**Figure 3c**). In the monodisperse emulsion stabilized by WPI, the concentration of lipid hydroperoxides and aldehydes increased slightly over the first four days and more rapidly between four and six days of incubation (**Figures 3a &b**). Similar effects were seen in the fluorescence intensity, which showed a minor decrease of red fluorescence in the first two days followed by a more rapid decrease between four and six days (**Figure 3c**). The decrease of red fluorescence was accompanied by the appearance of green fluorescence (excitation at 561 nm), confirming that the BODIPY 665/676 dye was getting oxidized (**Figure S8**). The simultaneous decrease in native (red) fluorescence and increase in hydroperoxides is in line with the formation of lipid peroxyl radicals in the droplets, leading to an increase in both lipid and BODIPY 665/676 oxidation[42,43] as we described in **Figure 2** with a kinetic model relating peroxyl radical formation to BODIPY 665/676 oxidation.

The formation of hydroperoxides and aldehydes in the colloid mill-made polydisperse emulsions stabilized by WPI proceeded faster than in monodisperse emulsions made with microfluidic devices (**Figure 3a & b**). Furthermore, we observed a clear difference between the decrease in red fluorescence emission for small (1-2 µm) and large droplets (4-5 µm) (**Figure 3c**). The faster lipid oxidation in small droplets compared to large ones is in line with our recent study, in which more lipid oxidation products are present in the smallest droplets present in the emulsions.[41] **Figure 3c** also indicated the decrease of the red fluorescence for 4-5 µm sized droplets in

monodisperse emulsions. The monodisperse droplets further showed a slower decrease over time than their similar-sized counterparts in the polydisperse emulsion. Several mechanisms can be envisaged to explain the difference in oxidation kinetics of similar (4-5 µm) sized droplets in emulsions manufactured with microfluidic and colloid mill emulsification. First, in a polydisperse emulsion the faster oxidation of small droplets (1-2 µm) can deplete oxygen required for oxidation of large droplets (4-5 µm) effectively leading to slower oxidation. Our model calculations show, however, that there should be enough O_2 present for large droplets to oxidize independently. Another potential mechanism is the colloidal transfer of oxidation intermediates formed in small droplets to larger ones. This mechanism can promote oxidation in large droplets especially in high oil-in-water emulsions with short distances between packed droplets. In our case, the oil fraction was only 15 wt.%, which is not in favour of effective mass transfer of oxidation intermediates between droplets. Thus, we arrive at the most likely explanation of a difference in the packing of WPI-proteins at the droplet interface introduced by mild and high shear emulsification. These differences in WPI packing have been observed previously in emulsions manufactured with different emulsification methods.[45] In that study, a higher concentration of proteins at the surface and a thicker interfacial layer could be seen by TEM in emulsions prepared with ultra-high-pressure homogenization compared to counterparts prepared by colloid mill and conventional homogenization.

Our comparison of local lipid oxidation in mono- and polydisperse emulsions pointed to a difference in packing of proteins at the droplet interfaces. We pursued this lead by further investigating the spatial, inter-droplet heterogeneity of lipid oxidation. Red fluorescence of BODIPY 665/676 in WPI-stabilized monodisperse emulsions showed clear inter-droplet heterogeneity in the oxidation of similar-sized droplets as quantified by standard deviations (shadowed areas in **Figure 3c**). This heterogeneity in fluorescence intensity levels confirms that for similar-sized WPI-stabilized droplets in a monodisperse emulsion, oxidation levels can differ greatly (**Figure 3d**).[46] We attribute this to the aforementioned heterogeneous coverage of droplet interfaces, which prompted us to further investigate the interplay of lipid and protein oxidation at droplet interfaces of WPI-stabilized emulsions with CLSM.

We note that when comparing local (microscopy) and bulk (^{1}H-NMR) assessments of lipid oxidation, one should consider the spatial resolution limit of the imaging technique used. In our CLSM experiments, the smallest droplets in which BODIPY 665/676 fluorescence could be quantified were ~ 1 µm in diameter. In our polydisperse WPI-stabilized emulsion, ~ 14 vol.% of the oil was present in droplets smaller than 1 µm and ~ 1 vol.% in droplets smaller than 0.2 µm, which represents the conventional resolution limit of CLSM. It was shown that more lipid oxidation products were present in the smallest droplets, which implies that lipid oxidation is underestimated if

only droplets larger than 1 µm are analyzed by CLSM.[41] The oxidation in tiny droplets could be further studied with super-resolution techniques which allow resolving features smaller than 200 nm.[47] We further note that a decrease in native fluorescence over time can also be caused by the dissolution of the dye into the continuous aqueous phase. Such an effect can occur when an emulsifier such as Tween 20 is present in a concentration high enough to dissolve the dye (**Figure S8**). Additionally, further attention is needed for using BODIPY 665/676 in protein stabilized food emulsions as many proteins such as bovine serum albumin (BSA) in WPI have some minor binding ability of lipids which can partly participate in transporting lipids.

3.4 Spatial heterogeneity of protein oxidation in WPI-stabilized emulsions

To further investigate the spatial inter- and intra-droplet heterogeneity of lipid and protein oxidation, we used CAMPO-AFDye 647[48] to localize protein radical formation and BODIPY 581/591 C11 for mapping lipid oxidation. This blue-shifted alternative BODIPY dye does not overlap with the emission of CAMPO-AFDye 647, which enabled us to co-localize protein and lipid oxidation. BODIPY 581/591 C11 has the same core structure as BODIPY 665/676 but contains only one phenylbutadiene moiety, which makes it less sensitive to lipid oxidation.[42,43] Co-localization of lipid and protein oxidation in polydisperse emulsions is shown in **Figure 4a** as overlayed raw image data. The image qualitatively shows that lipid oxidation indicated by BODIPY 581/591 C11 is accompanied by the accumulation of the CAMPO-AFDye 647 spintrap at the droplet interface. The distribution of spin traps is more closely visualised in the segmented droplets in poly- (**Figure 4b & c**) and monodisperse (**Figure 4d**) emulsions. The images of the colloid-mill made emulsion show spots of CAMPO-AFDye 647 accumulation at the interface, suggesting that proteins at the interface oxidize heterogeneously at both the inter- and intra-droplet level (**Figure 4b & c**). Heterogeneous protein distribution induced by colloid mill might make droplets more susceptible to lipid oxidation compared to the emulsions which have homogenous distribution of proteins at the interface. This finding could be explained by the heterogeneous interface of droplets featuring areas without proteins that could increase the chance of the lipids to react with AAPH in the aqueous phase.

For the monodisperse WPI-stabilized emulsions, only minor accumulation of CAMPO-AFDye 647 took place (**Figure 4d**). This finding indicates that little protein oxidation occurred at the interface, which we attribute to a more homogeneous protein coverage of the droplet interfaces due to the mildness of the microfluidic emulsification. In the panel in **Figure 4d** we can, however, still observe the droplet with enhanced BODIPY 581/591 C11 oxidation, accompanied with a spot of CAMPO-AFDye 647 accumulation at the interface. Hence also for the monodisperse droplets some inter-droplet heterogeneity exists for lipid and protein oxidation, which is also in line with **Figure 3**. The co-localization of protein and lipid oxidation in monodisperse emulsions suggests

that protein oxidation is initiated by lipid oxidation. However, given the use of the AAPH initiator, we cannot exclude that this agent directly attacks proteins at the interface. We also note that there is a possibility that the fluorescence signals from the homogeneous thin protein layer in monodisperse emulsions might be not able to provide sufficient signal for CLSM measurements.

To quantify the interplay between protein- and lipid oxidation at the intra-droplet level, we first determined the average fluorescence intensity from BODIPY 581/591 C11. Next, we integrated the fluorescence by CAMPO-AFDye 647 and divided the value by the circumference ($2\pi r$) with the calculated radius r from the segmentation to obtain a measure for protein oxidation at the interface. This quantification revealed heterogeneity for lipid oxidation (**Figure 4e**), as discussed earlier (**Figure 3c & d**) and also for protein oxidation (**Figure 4f**). In polydisperse emulsions, both lipid and protein showed more oxidation for smaller droplets. This droplet size dependency is, however, more pronounced for lipid as for protein oxidation.

To sum up, in WPI-stabilized emulsions, both lipid and protein oxidation at the interface occurred faster in the polydisperse emulsion than in the monodisperse one (**Figures 3a & b** and **4c & d**). This finding can be explained by both the differences in the emulsification process and the presence of smaller droplets, as we described in the previous section. Thus, our results can help to explain ambiguous outcomes of previous studies on the droplet size dependency of lipid oxidation, as different emulsification methods can lead to different droplet surface coverage and/or droplet size distributions.[49,50] Unfortunately, our current data do not provide clear evidence of protein oxidation induced by lipid oxidation. Both oxidation mechanisms may occur independently, or the oxidation initiator (AAPH) does not only promote lipid oxidation but also protein oxidation at the interface.

4 Conclusions

In this study, the intensity decrease in red fluorescence emission of BODIPY 665/676 was used to unravel droplet size-dependent spatial heterogeneity of lipid oxidation in WPI-stabilized emulsions. By modelling the kinetic rates of underlying lipid oxidation reactions, we showed that no perturbation of lipid oxidation occurs at the chosen low concentration of BODIPY 665/676. The kinetic model inferred that the decrease in red fluorescence of BODIPY 665/676 correlates with the increase of integrated peroxyl radical concentration over time. Microfluidic and colloid mill emulsification respectively result in mono- and polydisperse WPI emulsions. Kinetic curves of oxidation products of these oxidized emulsions, as observed locally by BODIPY 665/676 and in bulk by ^{1}H-NMR, can be explained by differences in droplet size distribution and heterogeneous packing of proteins at the droplet interfaces (**Figure 5**). The different packing of proteins at the droplet interfaces of mono- and polydisperse WPI emulsions

could be visualized by the accumulation of the CAMPO-AFDye 647 spin trap at droplet interfaces. Our results show that both lipid and protein oxidation proceed in highly heterogeneous fashion in WPI-stabilized emulsions, which cannot be derived from bulk measurements of lipid oxidation products. We expect that our work will contribute to improving the understanding of local co-oxidation of lipids and proteins at droplet interfaces.

Funding Statement

This work was financially supported by the Netherlands Organisation for Scientific Research (NWO) in the framework of the Innovation Fund for Chemistry and from the Ministry of Economic Affairs in the framework of the 'TKI/PPS-Toeslagregeling', with Grant No. of 731.017.301.

CRediT authorship contribution statement

Suyeon Yang: Investigation, Validation, Visualization, Writing - original draft. **Sten ten Klooster**: Investigation, Validation, Visualization, Writing - original draft. **Khoa A. Nguyen**: Software, Formal analysis, Investigation, Writing-review & editing. **Marie Hennebelle**: Investigation, Writing-review & editing. **Claire Berton-Carabin**: Investigation, Writing-review & editing. **Karin Schroën**: Investigation, Writing-review & editing. **John P.M. van Duynhoven**: Conceptualization, Supervision, Writing - review & editing, Funding acquisition. **Johannes Hohlbein**: Conceptualization, Supervision, Writing - review & editing, Funding acquisition.

Declaration of Competing Interest

J.P.M.v.D. is employed by a company that manufactures and markets mayonnaise. The other authors declare that they have no known competing financial interests or personal relationships that could influence the work reported in this paper.

Acknowledgments

We would like to thank our colleagues in the LICENSE consortium for helpful discussions.

Table 1. The summary of lipid oxidation reactions that can occur at the water-oil interface in O/W food emulsions.

Lipid oxidation reactions	
$LH \xrightarrow{k_1} L^* + H^*$	R.1
$L^* + O_2 \xrightarrow{k_2} LOO^*$	R.2
$LOO^* + LH \xrightarrow{k_3} LOOH + L^*$	R.3
$LOOH \xrightarrow{k4} LO^* + OH^*$	R.4
$OH^* + LH \xrightarrow{k_5} L^* + H_2O$	R.5
$LO^* + LH \xrightarrow{k_6} AD + L^*$	R.6*
$LO^* + LH \xrightarrow{k_7} EP + L^*$	R.7*
Reactions in the presence of AAPH and BODIPY	
$AAPH \xrightarrow{k_{AAPH}} 2L^* + N_2$	R.8
$LOO^* + BODIPY \xrightarrow{k_{BODIPY}}$ non-radical products	R.9

*R.6-R.7 results from the combination of multi-chain reactions to form aldehydes, epoxides, and EPOOHs.[34]

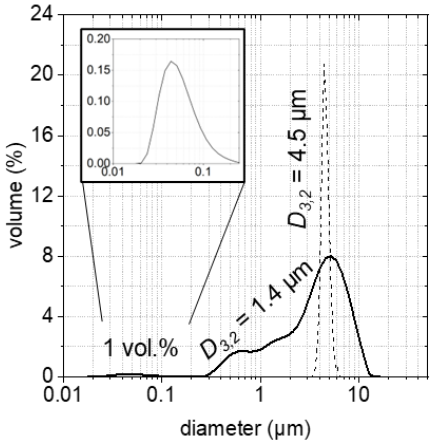

Figure 1. Distribution of the volume fraction per diameter of emulsions stabilized with WPI. The solid line represents emulsions prepared with the colloid mill, and the dashed line with microfluidics. The droplet size distribution for the colloid mill-made emulsion were obtained by combining the SLS results on the whole emulsion sample with the DLS results on the subnatant sample obtained after centrifugation (**section 2.5**). The D_{32} values were obtained from the CLSM results for the microfluidic-made emulsions and from SLS and DLS for the colloid mill-made emulsions. The volume fraction of tiny droplets (D_{32} < 200 nm) in WPI emulsions is 1 % v/v (subset).

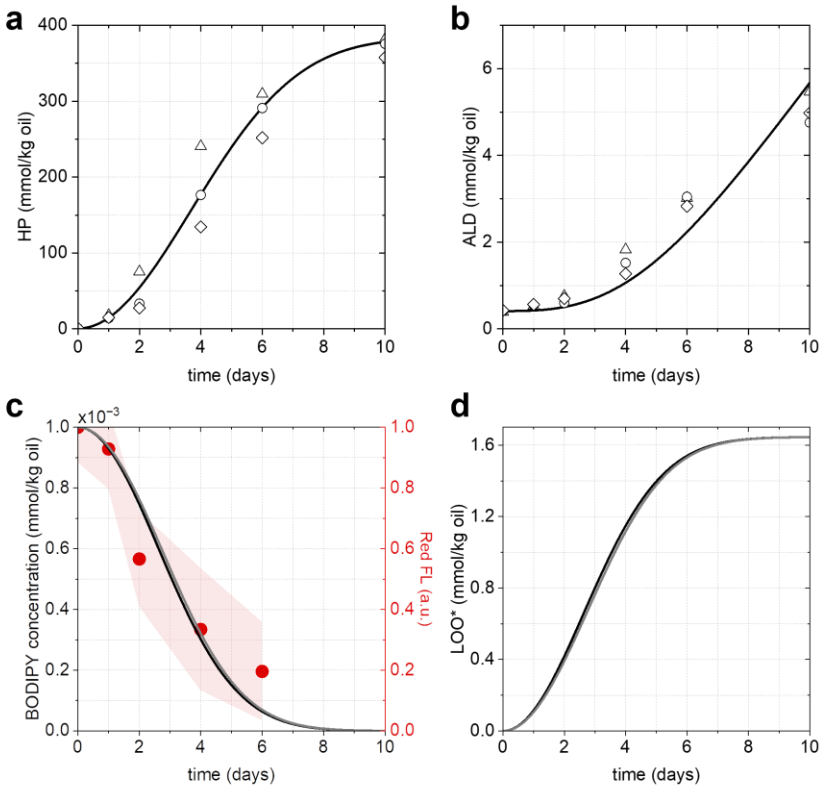

Figure 2. Validation of using BODIPY 665/676 to probe oxidation by experimental and simulated data. (**a-b**) The formation of hydroperoxides (HP) (a) and aldehydes (ALD) (b) in the absence and presence of BODIPY 665/676 as measured by ^{1}H-NMR. The samples were prepared with a colloid mill (polydisperse emulsions) and stabilized by 2 wt.% WPI. Markers corresponding to samples containing 0 (triangle), 1 (circle), and 50 µM (diamond) BODIPY 665/676. The black line indicates the numerical datasets (simulation) of total HP and ALD. Note that the simulation results from 0, 1, and 50 µM showed no differences, whereas the experimental results showed differences, which we attributed to the differences in droplet size distribution between the sample production (**Figure S6**). (**c**) Correlation between experimental (fluorescence intensity) and simulation data (BODIPY 665/676 concentration) with 1 µM BODIPY 665/676. (Left y-axis) Solid lines indicate the concentration of native BODIPY 665/676 calculated from **Equation 6** (black) and **7** (grey). (Right y-axis) Red circles indicate the intensity decrease of red fluorescence. Shadow areas denote the standard deviations of many droplets from two independently incubated samples. We note that the large standard deviation originates from many droplets in the range of 1 - 6 µm diameter. More than 2000 oil droplets were used for the analyses at each time point. (**d**) Simulated results of LOO* concentration which reacts with BODIPY 665/676. Lines show the integration term divided by the constant (k_{BODIPY}) in **Equation 6** (black) and the approximated concentration of LOO* in **Equation 7** (gray).

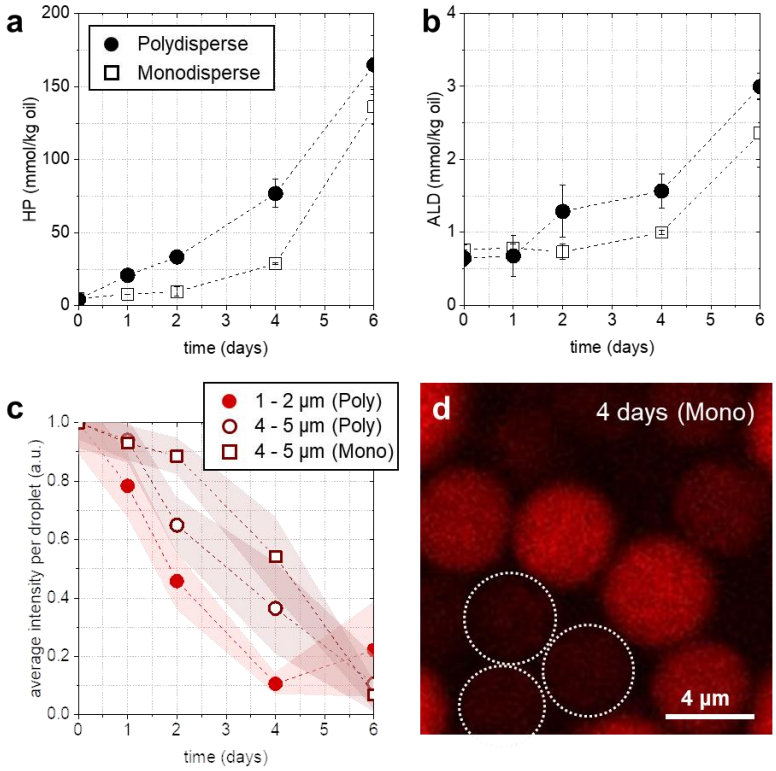

Figure 3. Lipid oxidation in colloid mill-made polydisperse (filled-circle) or in microfluidic-made monodisperse (empty square) emulsions stabilized by 2 wt.% WPI. (**a-b**) Formation of hydroperoxides (HP) (a) and aldehydes (ALD) (b) as a function of time measured by ^{1}H-NMR. Error bars (sometimes hidden within the symbol) denote standard deviations of four measurements including two independent sample preparations. The result indicates that polydisperse emulsions showed faster oxidation than monodisperse emulsions. (**c**) Decrease of red fluorescence by BODIPY 665/676 in poly- and monodisperse emulsions. Symbols in c correspond to droplet sizes of 1-2 µm (filled-circle, red) and 4-5 µm (empty-circle, dark red) from the polydisperse emulsions and 4-5 µm (empty square, dark red) sized-droplets in the monodisperse system. Shadow areas denote the standard deviations of many droplets from two independently incubated samples. The dashed lines connecting the average values are for visual guidance. (**d**) CLSM image of WPI-stabilized monodisperse emulsions after four days of oxidation, indicating inter-droplet heterogeneity of lipid oxidation.

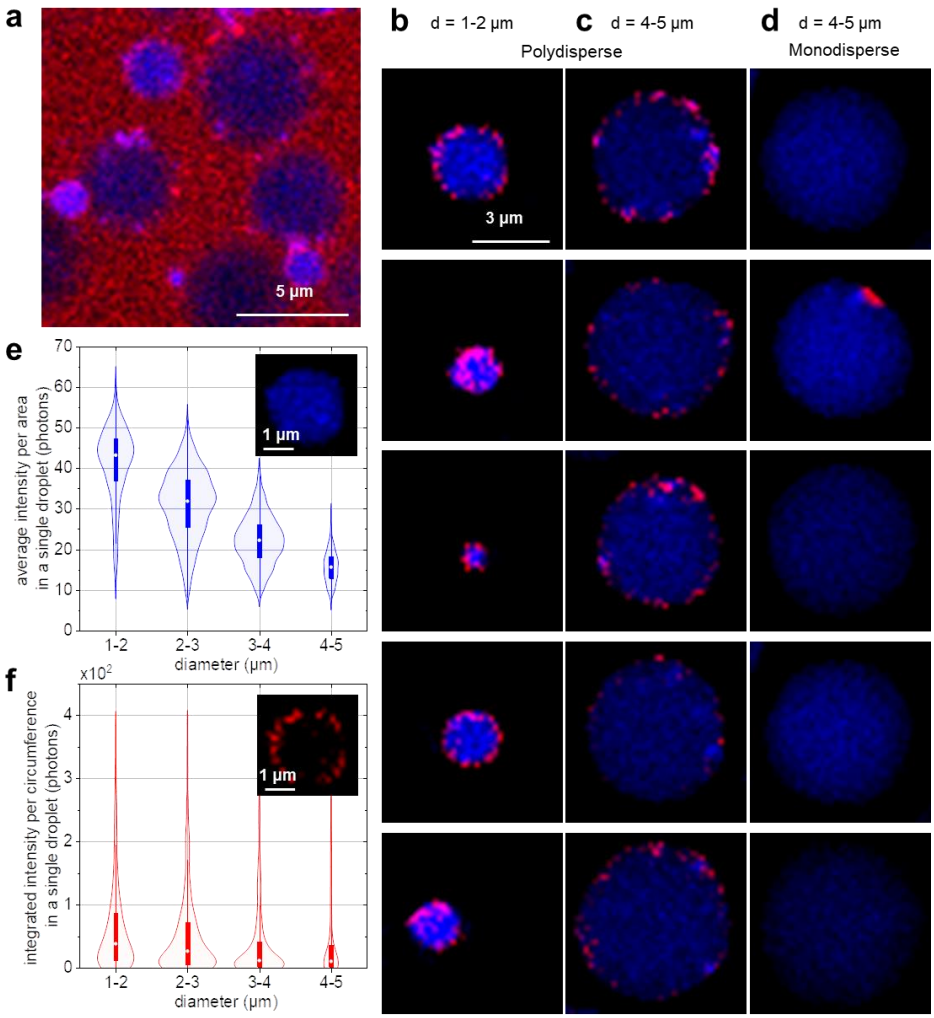

Figure 4. Imaging the heterogeneity of lipid and protein oxidation in mono- and polydisperse emulsions stabilized by WPI. Co-localization of lipid and protein oxidation was assessed using BODIPY 581/591 C11 (excitation at 488 nm for the oxidized droplets) and CAMPO-AFDye 647 (excitation at 640 nm). (**a**) Raw image data of colloid mill-made emulsions with combined excitation channels at 488- and 640 nm. The red colour shows the accumulation of CAMPO-AFDye 647, and the blue indicates lipid oxidation. (b-d) Representative segmented droplet images showing lipid and protein oxidation with emulsions prepared in a colloid mill in two different size ranges of droplets (1-2 µm and 4-5 µm) (**b** and **c**) or a microfluidic device (**d**). (e-f) Droplet size dependency of lipid- (**e**) and protein oxidation (**f**) in polydisperse emulsions. Quantification steps were performed as described in section 2.4. As we took the data from a single measurement set, we did not perform a normalization step (**Figure S3**). The subset figure in (e) and (f) indicates the segmented images of oil droplets with BODIPY 581/591 C11 and interface with CAMPO-AFDye 647 in polydisperse emulsions, respectively. The box plot shows the data in the 25 to 75 % range, and the white circle in the box plot shows the median value. The numbers of analysed droplets for diameters (d) in the ranges $1 \leq d < 2$, $2 \leq d < 3$, $3 \leq d < 4$, and $4 \leq d < 5$ µm are 764, 1205, 1046, and 305, respectively.

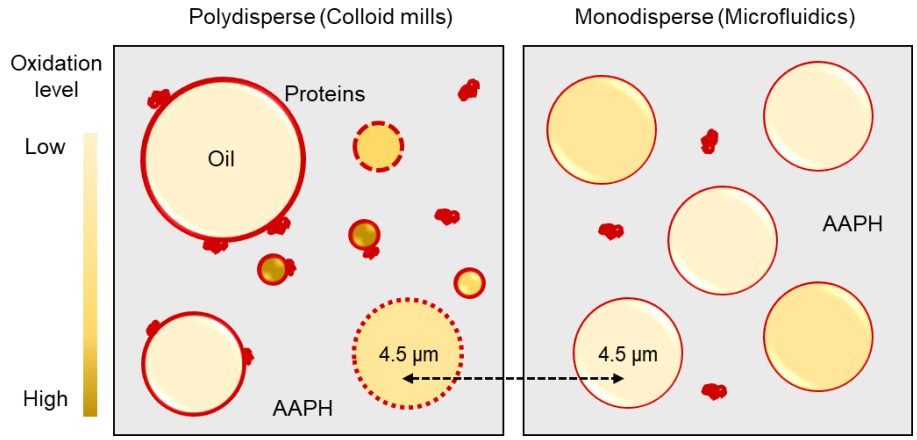

Figure 5. Schematic overview of the findings in this study. Colloid mills and microfluidic emulsification respectively result in poly- and monodisperse emulsions, respectively. Left, In polydisperse emulsions, droplets are heterogeneously covered with proteins. Right, In monodisperse emulsions, the coverage is homogeneous. The black dashed line connects similar (4-5 µm) sized droplets that differ in surface coverage and protein and lipid oxidation behaviour.

References

(1) McClements, D. J.; Decker, E. A. Lipid Oxidation in Oil-in-Water Emulsions: Impact of Molecular Environment on Chemical Reactions in Heterogeneous Food Systems. *J Food Sci* **2000**, *65* (8), 1270–1282. https://doi.org/10.1111/j.1365-2621.2000.tb10596.x.

(2) McClements, D. J. *Food Emulsions: Principles, Practices, and Techniques*; CRC press, 2015.

(3) Berton-Carabin, C. C.; Ropers, M. H.; Genot, C. Lipid Oxidation in Oil-in-Water Emulsions: Involvement of the Interfacial Layer. *Compr Rev Food Sci Food Saf* **2014**, *13* (5), 945–977. https://doi.org/10.1111/1541-4337.12097.

(4) Joint, F. A. O. Fats and Fatty Acids in Human Nutrition. Report of an Expert Consultation, 10-14 November 2008, Geneva. **2010**.

(5) Vannice, G.; Rasmussen, H. Position of the Academy of Nutrition and Dietetics: Dietary Fatty Acids for Healthy Adults. *J Acad Nutr Diet* **2014**, *114* (1), 136–153.

(6) Schaich, K. M. Challenges in Elucidating Lipid Oxidation Mechanisms: When, Where, and How Do Products Arise? In *Lipid oxidation*; Elsevier, 2013; pp 1–52.

(7) Kerr, J. A. Bond Dissociation Energies by Kinetic Methods. *Chem Rev* **1966**, *66* (5), 465–500.

(8) Frankel, E. N.; Meyer, A. S. The Problems of Using One-Dimensional Methods to Evaluate Multifunctional Food and Biological Antioxidants. *J Sci Food Agric* **2000**, *80* (13), 1925–1941. https://doi.org/10.1002/1097-0010(200010)80:13<1925::AID-JSFA714>3.0.CO;2-4.

(9) Abeyrathne, E. D. N. S.; Nam, K.; Ahn, D. U. Analytical Methods for Lipid Oxidation and Antioxidant Capacity in Food Systems. *Antioxidants 2021, Vol. 10, Page 1587* **2021**, *10* (10), 1587. https://doi.org/10.3390/ANTIOX10101587.

(10) Zhang, Y.; Wang, M.; Zhang, X.; Qu, Z.; Gao, Y.; Li, Q.; Yu, X. Mechanism, Indexes, Methods, Challenges, and Perspectives of Edible Oil Oxidation Analysis. *https://doi.org/10.1080/10408398.2021.2009437* **2021**. https://doi.org/10.1080/10408398.2021.2009437.

(11) Villeneuve, P.; Bourlieu-Lacanal, C.; Durand, E.; Lecomte, J.; McClements, D. J.; Decker, E. A. Lipid Oxidation in Emulsions and Bulk Oils: A Review of the Importance of Micelles. *Critical Reviews in Food Science and Nutrition*. Taylor and Francis Ltd. 2021. https://doi.org/10.1080/10408398.2021.2006138.

(12) Laguerre, M.; Tenon, M.; Bily, A.; Birtić, S. Toward a Spatiotemporal Model of Oxidation in Lipid Dispersions: A Hypothesis-Driven Review. *European Journal of Lipid Science and Technology* **2020**, *122* (3), 1900209.

(13) Li, P.; McClements, D. J.; Decker, E. A. Application of Flow Cytometry as Novel Technology in Studying the Effect of Droplet Size on Lipid Oxidation in Oil-in-Water Emulsions. *J Agric Food Chem* **2019**, *68* (2), 567–573.

(14) Li, P.; McClements, D. J.; Decker, E. A. Application of Flow Cytometry as Novel Technology in Studying Lipid Oxidation and Mass Transport Phenomena in Oil-in-Water Emulsions. *Food Chem* **2020**, *315*, 126225.

(15) Banerjee, C.; Breitenbach, T.; Ogilby, P. R. Spatially Resolved Experiments to Monitor the Singlet Oxygen Initiated Oxidation of Lipid Droplets in Emulsions. *ChemPhotoChem* **2018**, *2* (7), 586–595.

(16) Yang, S.; Verhoeff, A. A.; Merkx, D. W. H.; van Duynhoven, J. P. M.; Hohlbein, J. Quantitative Spatiotemporal Mapping of Lipid and Protein Oxidation in Mayonnaise. *Antioxidants* **2020**, *9* (12), 1–13. https://doi.org/10.3390/antiox9121278.

(17) Boens, N.; Leen, V.; Dehaen, W. Fluorescent Indicators Based on BODIPY. *This journal is Cite this: Chem. Soc. Rev* **2012**, *41*, 1130–1172. https://doi.org/10.1039/c1cs15132k.

(18) Banerjee, C.; Breitenbach, T.; Ogilby, P. R. Spatially Resolved Experiments to Monitor the Singlet Oxygen Initiated Oxidation of Lipid Droplets in Emulsions. *ChemPhotoChem* **2018**, *2* (7), 586–595. https://doi.org/10.1002/CPTC.201800005.

(19) Raudsepp, P.; Brüggemann, D. A.; Andersen, M. L. Evidence for Transfer of Radicals between Oil-in-Water Emulsion Droplets as Detected by the Probe (E, E)-3, 5-Bis (4-Phenyl-1, 3-Butadienyl)-4, 4-Difluoro-4-Bora-3a, 4a-Diaza-s-Indacene, BODIPY665/676. *J Agric Food Chem* **2014**, *62* (51), 12428–12435.

(20) Raudsepp, P.; Brüggemann, D. A.; Knudsen, J. C.; Andersen, M. L. Localized Lipid Autoxidation Initiated by Two-Photon Irradiation within Single Oil Droplets in Oil-in-Water Emulsions. *Food Chem* **2016**, *199*, 760–767.

(21) ten Klooster, S.; Schroën, K.; Berton-Carabin, C. Lipid Oxidation Products in Model Food Emulsions: Do They Stay in or Leave Droplets, That's the Question. *Food Chem* **2022**, 134992.

(22) Berton, C.; Genot, C.; Ropers, M. Journal of Colloid and Interface Science Quantification of Unadsorbed Protein and Surfactant Emulsifiers in Oil-in-Water Emulsions. *J Colloid Interface Sci* **2011**, *354* (2), 739–748. https://doi.org/10.1016/j.jcis.2010.11.055.

(23) ten Klooster, S.; Berton-Carabin, C.; Schroën, K. Design Insights for Upscaling Spontaneous Microfluidic Emulsification Devices Based on Behavior of the Upscaled Partitioned EDGE Device. *Food Research International* **2022**, 112365.

(24) Cuvelier, M.-E.; Soto, P.; Courtois, F.; Broyart, B.; Bonazzi, C. Oxygen Solubility Measured in Aqueous or Oily Media by a Method Using a Non-Invasive Sensor. *Food Control* **2017**, *73*, 1466–1473.

(25) Truesdale, G. A.; Downing, A. L.; Lowden, G. F. The Solubility of Oxygen in Pure Water and Sea-water. *Journal of Applied Chemistry* **1955**, *5* (2), 53–62.

(26) Srinivasan, S.; Xiong, Y. L.; Decker, E. A. Inhibition of Protein and Lipid Oxidation in Beef Heart Surimi-like Material by Antioxidants and Combinations of PH, NaCl, and Buffer Type in the Washing Media. *J Agric Food Chem* **1996**, *44* (1), 119–125.

(27) Shantha, N. C.; Decker, E. A. Rapid, Sensitive, Iron-Based Spectrophotometric Methods for Determination of Peroxide Values of Food Lipids. *J AOAC Int* **1994**, *77* (2), 421–424.

(28) Ten Klooster, S.; Villeneuve, P.; Bourlieu-Lacanal, C.; Durand, E.; Schroën, K.; Berton-Carabin, C. Alkyl Chain Length Modulates Antioxidant Activity of Gallic Acid Esters in Spray-Dried Emulsions. *Food Chem* **2022**, *387*, 132880.

(29) Merkx, D. W. H.; Hong, G. T. S.; Ermacora, A.; Van Duynhoven, J. P. M. Rapid Quantitative Profiling of Lipid Oxidation Products in a Food Emulsion by 1H NMR. *Anal Chem* **2018**, *90* (7), 4863–4870. https://doi.org/10.1021/acs.analchem.8b00380.

(30) Schmidt, U.; Weigert, M.; Broaddus, C.; Myers, G. *Cell Detection with Star-Convex Polygons*; 2018; Vol. 11071 LNCS. https://doi.org/10.1007/978-3-030-00934-2_30.

(31) ten Klooster, S.; Takeuchi, M.; Schroën, K.; Tuinier, R.; Joosten, R.; Friedrich, H.; Berton-Carabin, C. Tiny, yet Impactful: Detection and Oxidative Stability of Very Small Oil Droplets in Surfactant-Stabilized Emulsions. *J Colloid Interface Sci* **2023**, *652*, 1994–2004. https://doi.org/10.1016/J.JCIS.2023.09.005.

(32) Jacobs, N. J.; Vandenmark, P. J. Colorimetric Method for Determination of Triglycsrides. *Arch Biochem. Biophys* **1960**, *88*, 250–255.

(33) Trinder, P. Quantitative Determination of Triglyceride Using GPO-PAP Method. *Ann Biochem* **1969**, *6*, 24–27.

(34) Nguyen, K. A.; Hennebelle, M.; van Duynhoven, J. P. M.; Dubbelboer, A.; Boerkamp, V. J. P.; Wierenga, P. A. Mechanistic Kinetic Modelling of Lipid Oxidation in Vegetable Oils to Estimate Shelf-Life. *Food Chem* **2024**, *433*, 137266. https://doi.org/10.1016/J.FOODCHEM.2023.137266.

(35) van Boekel, M. A. J. S. Kinetic Modeling of Reactions In Foods. *Kinetic Modeling of Reactions In Foods* **2008**. https://doi.org/10.1201/9781420017410.

(36) Muñoz-Tamayo, R.; de Groot, J.; Bakx, E.; Wierenga, P. A.; Gruppen, H.; Zwietering, M. H.; Sijtsma, L. Hydrolysis of β-Casein by the Cell-Envelope-Located PI-Type Protease of Lactococcus Lactis: A Modelling Approach. *Int Dairy J* **2011**, *21* (10), 755–762. https://doi.org/10.1016/j.idairyj.2011.03.012.

(37) Yoshida, Y.; Shimakawa, S.; Itoh, N.; Niki, E. Action of DCFH and BODIPY as a Probe for Radical Oxidation in Hydrophilic and Lipophilic Domain. *Free Radic Res* **2003**, *37* (8), 861–872. https://doi.org/10.1080/1071576031000148736.

(38) Takahashi, A.; Shibasaki-Kitakawa, N.; Noda, T.; Sukegawa, Y.; Kimura, Y.; Yonemoto, T. Kinetic Analysis of Co-Oxidation of Biomembrane Lipids Induced by Water-Soluble Radicals. *JAOCS, Journal of the American Oil Chemists' Society* **2016**, *93* (6), 803–811. https://doi.org/10.1007/s11746-016-2821-x.

(39) Schroën, K.; Berton-Carabin, C. C. A Unifying Approach to Lipid Oxidation in Emulsions: Modelling and Experimental Validation. *Food Research International* **2022**, *160* (March). https://doi.org/10.1016/j.foodres.2022.111621.

(40) van Boekel, M. A. J. S. Kinetic Modeling of Reactions In Foods. *Kinetic Modeling of Reactions In Foods* **2008**. https://doi.org/10.1201/9781420017410.

(41) Klooster, S. ten; Schroën, K.; Berton-Carabin, C. Lipid Oxidation Products in Model Food Emulsions: Do They Stay in or Leave Droplets, That's the Question. *Food Chem* **2023**, *405* (November 2022). https://doi.org/10.1016/j.foodchem.2022.134992.

(42) Naguib, Y. M. A. Antioxidant Activities of Astaxanthin and Related Carotenoids. *J Agric Food Chem* **2000**, *48* (4), 1150–1154.

(43) Raudsepp, P.; Brüggemann, D. A.; Andersen, M. L. Detection of Radicals in Single Droplets of Oil-in-Water Emulsions with the Lipophilic Fluorescent Probe BODIPY665/676 and Confocal Laser Scanning Microscopy. *Free Radic Biol Med* **2014**, *70*, 233–240.

(44) Drummen, G. P. C.; Gadella, B. M.; Post, J. A.; Brouwers, J. F. Mass Spectrometric Characterization of the Oxidation of the Fluorescent Lipid Peroxidation Reporter Molecule C11-BODIPY581/591. *Free Radic Biol Med* **2004**, *36* (12), 1635–1644. https://doi.org/10.1016/j.freeradbiomed.2004.03.014.

(45) Hebishy, E.; Buffa, M.; Guamis, B.; Blasco-Moreno, A.; Trujillo, A. J. Physical and Oxidative Stability of Whey Protein Oil-in-Water Emulsions Produced by Conventional and Ultra High-Pressure Homogenization: Effects of Pressure and Protein Concentration on Emulsion Characteristics. *Innovative Food Science and Emerging Technologies* **2015**, *32* (October 2015), 79–90. https://doi.org/10.1016/j.ifset.2015.09.013.

(46) Berton, C.; Ropers, M. H.; Guibert, D.; Solé, V.; Genot, C. Modifications of Interfacial Proteins in Oil-in-Water Emulsions Prior to and during Lipid Oxidation. *J Agric Food Chem* **2012**, *60* (35), 8659–8671. https://doi.org/10.1021/jf300490w.

(47) Hohlbein, J. Single-Molecule Localization Microscopy as an Emerging Tool to Probe Multiscale Food Structures. *Food Structure* **2021**, *30*, 100236. https://doi.org/10.1016/J.FOOSTR.2021.100236.

(48) Yang, S.; Takeuchi, M.; Friedrich, H.; van Duynhoven, J. P. M.; Hohlbein, J. Unravelling Mechanisms of Protein and Lipid Oxidation in Mayonnaise at Multiple Length Scales. *Food Chem* **2023**, *402*, 134417. https://doi.org/10.1016/J.FOODCHEM.2022.134417.

(49) Neves, M. A.; Wang, Z.; Kobayashi, I.; Nakajima, M. Assessment of Oxidative Stability in Fish Oil-in-Water Emulsions: Effect of Emulsification Process, Droplet Size and Storage Temperature. *J Food Process Eng* **2017**, *40* (1), e12316. https://doi.org/10.1111/JFPE.12316.

(50) Atarés, L.; Marshall, L. J.; Akhtar, M.; Murray, B. S. Structure and Oxidative Stability of Oil in Water Emulsions as Affected by Rutin and Homogenization Procedure. *Food Chem* **2012**, *134* (3), 1418–1424. https://doi.org/10.1016/J.FOODCHEM.2012.02.221.

Supplementary Materials:

Droplet size dependency and spatial heterogeneity of lipid oxidation in whey protein isolate-stabilized emulsions

Suyeon Yang[a,1], Sten ten Klooster[b,1], Khoa A. Nguyen[c], Marie Hennebelle[c], Claire Berton-Carabin[b,d], Karin Schroën[b], John P.M. van Duynhoven[a,e,*], Johannes Hohlbein[a,f,*]

[a] Laboratory of Biophysics, Wageningen University & Research, Stippeneng 4, 6708 WE Wageningen, the Netherlands

[b] Laboratory of Food Process Engineering, Wageningen University & Research, 6708 WG, Wageningen, The Netherlands

[c] Laboratory of Food Chemistry, Wageningen University & Research, 6708 WG, Wageningen, The Netherlands

[d] INRAE, UR BIA, 44300 Nantes, France

[e] Unilever Global Foods Innovation Centre, Plantage 14, 6708 WJ Wageningen, the Netherlands

[f] Microspectroscopy Research Facility, Wageningen University & Research, Stippeneng 4, 6708 WE Wageningen, the Netherlands

[1] These authors contributed equally.

[*] Corresponding authors: john.vanduynhoven@wur.nl (John P.M. van Duynhoven), johannes.hohlbein@wur.nl (Johannes Hohlbein).

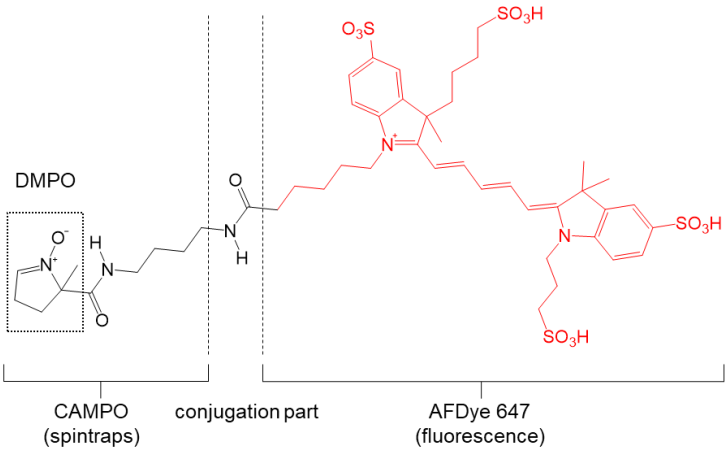

Figure S1. The chemical structure of fluorescently labelled spin traps (CAMPO-AFDye 647). CAMPO, which is a derivate of DMPO, is conjugated with the fluorescent dye, AFDye 647.

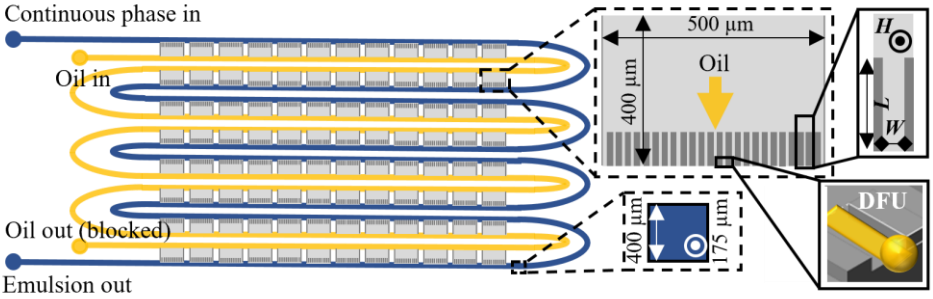

Figure S2. Top-view design of the Upscaled Partitioned EDGE chips used in this research to generate monodisperse droplet emulsions. The blue 'twisted road' channel represents the continuous aqueous-phase channel. The yellow 'twisted road' channel represents the to-be-dispersed oil-phase channel. The gray rectangular areas between these channels are the main plateaus containing 24 micro-plateaus of 50 x 10 x 1 µm (L x W x H) with the droplet formation units (DFU). A 3D representation of a DFU is shown in the right lower corner, showing oil – in yellow – being pushed out of the DFU and forming a droplet ready to detach. This illustration is not to scale; only 12 out of the 42 main plateaus are shown per row.

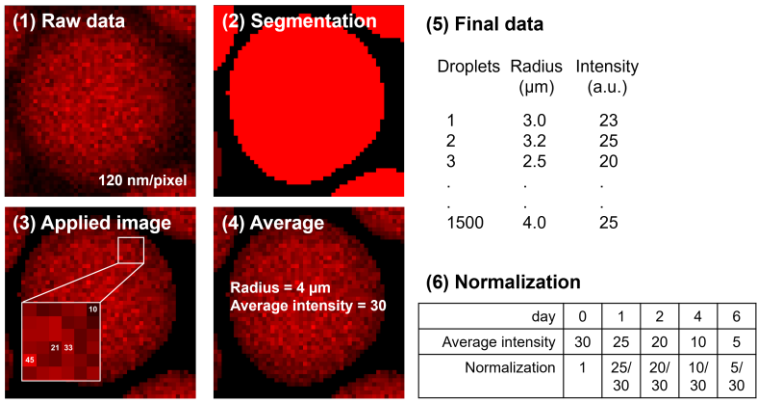

Figure S3. Data analysis pathway of microscopy images. (**1**) Raw image data (excited at 640 nm) were acquired using CLSM as described in the main text (**section 2.3.5**). The pixel size was 120 nm (512 x 512 pixels providing a 61.4 x 61.4 µm wide field of view). (**2**) The segmentation masks of oil droplets were acquired by applying 2D StarDist to the sum of the green and red detection channels (ex 561 + ex 640 nm). (**3**) Then, masks and raw data were multiplied using MATLAB. (**4**) The average intensity of each droplet was used for further analyses, and the radius of the droplet was calculated from the number of pixels with the assumption of circle shape; r (radius, µm) = $0.12 \cdot \sqrt{(\text{Sum of pixel numbers} / \pi)}$, 1 pixel = 0.12 µm. (**5**) Finally, we obtained a list of droplet numbers and radii with the average intensity per droplet. (**6**) To compare data obtained under different conditions over different days, the initial intensity was set to 1, and all other data points were divided by the average intensity of all droplets at day 0.

Table S1: Kinetic rates of underlying lipid oxidation reactions in the O/W emulsions with the presence of AAPH and BODIPY

$\frac{d[L*]}{dt} = k_1[LH] - k_2[L^*][O2] + k_3[LOO^*][LH] + k_5[OH^*][LH] + k_6[LO^*][LH] + k_7[LO^*][LH] + 0.5k_{AAPH}[AAPH]$	eq.S1
$\frac{d[LH]}{dt} = -k_1[LH] - k_3[LOO^*][LH] - k_5[OH^*][LH] - k_6[LO^*][LH] - k_7[LO^*][LH]$	eq.S2
$\frac{d[LOO^*]}{dt} = k_2[L^*][O2] - k_3[LOO^*][LH] - k_{BODIPY}[LOO^*][BODIPY]$	eq.S3
$\frac{d[O2]}{dt} = -k_2[L^*][O2]$	eq.S4
$\frac{d[LO^*]}{dt} = k_4[LOOH] - k_6[LO^*][LH] - k_7[LO^*][LH]$	eq.S5
$\frac{d[LOOH]}{dt} = k_3[LOO^*][LH] - k_4[LOOH]$	eq.S6
$\frac{d[AD]}{dt} = k_6[LO^*][LH]$	eq.S7
$\frac{d[EP]}{dt} = k_7[LO^*][LH]$	eq.S8
$\frac{d[AAPH]}{dt} = -k_{AAPH}[AAPH]$	eq.S9
$\frac{d[BODIPY]}{dt} = -k_{BODIPY}[LOO^*][BODIPY]$	eq.S10
$\frac{d[OH^*]}{dt} = k_4[LOOH] - k_5[OH^*][LH]$	eq.S11

Table S2: Estimated values versus literature values of model kinetic constants at 25 °C

Parameters	Estimated values[(1)]	Lower and upper bounds of starting values[(2)]	Literature values
k_1 (s^{-1})	2.09×10^{-8}	$[10^{-15},10^{-5}]$	$\sim10^{-15}$ [1,2]
k_2 ($mol^{-1}.m^3.s^{-1}$)	1.026×10^{-7}	$[10^{-15}, 100]$	100 at 37°C [3]
k_3 ($mol^{-1}.m^3.s^{-1}$)	3.04×10^{-7}	$[10^{-15}, 10^{-3}]$	10^{-4} to 10^{-3} at 40°C [2,4]
k_4 (s^{-1})	2.7×10^{-8}	$[10^{-15}, 10^{-2}]$	10^{-3}
k_5 ($mol^{-1}.m^3.s^{-1}$)	5×10^{-6}	$[10^{-15}, 10^{3}]$	--
k_6 ($mol^{-1}.m^3.s^{-1}$)	10^2	$[10^{-5}, 10^{3}]$	10^{-5} to 10^{-2} at 20°C [5]
k_7 ($mol^{-1}.m^3.s^{-1}$)	0.3	$[10^{-5}, 10]$	0.032 to 3.3 [5]
k_{AAPH} (s^{-1})	3.75×10^{-10}	$[10^{-15}, 10^{-6}]$	10^{-7} to 10^{-6} at 40°C [2]
k_{BODIPY} ($mol^{-1}.m^3.s^{-1}$)	6.08×10^{-7}	$[2\times10^{-15}, 2\times10^{-3}]$	$2\times k_3$ [6] or 6×10^{-3} $M^{-1}s^{-1}$ at 37 °C [(3)]
Initial concentration of lipid radicals (mol/m^3 oil)[(4)]	10^{-11}	$[10^{-15}, 10^{-9}]$	2×10^{-12} (L*), 10^{-13} (LOO*), 7×10^{-18} (OH*) [7]

[(1)]The deviations of the estimated values < 1% from 200 iteration Monte Carlo simulations, indicating that the optimization is robust enough for the estimation of the kinetic constants and initial radical concentrations; [(2)]We cut off the upper bound of starting values if their excess values return significantly higher residuals than the previous fitting tests. [(3)]As far as we know, there is only one report about the kinetic constant of another BODIPY type (BODIPY 581/591 C11), but not BODIPY 665/676. [(4)]These (estimated) initial radical concentrations were determined through many tests of global optimisation. Following this, our outputs did not change when we only changed radical concentrations within the given bounds and kept the estimated values of the rest parameters. This illustrated that these radical values within the lower and upper bounds were not sensitive to the output.

Partition coefficients of O_2 and AAPH at water-oil interfaces

The changes in O_2 and AAPH from different droplet sizes are quantitatively considered in K as a partition coefficient that depends on droplet sizes. For instance, the concentration of O_2 at the water-oil interface in accordance with changes in droplet sizes was calculated (eq.S12).

$$[O_2]_O = K\frac{V_W}{V_O}[O_2]_W = K\frac{V_W}{V_O(D_{32})}[O_2]_W \quad \text{eq.S12}$$

$$[\widetilde{O}_2]_O = K\frac{V_W}{V_O(\widetilde{D}_{32})}[O_2]_W \text{ where } \widetilde{D}_{32} = D_{32} \pm \sigma \quad \text{eq.S13}$$

$$\frac{[\widetilde{O}_2]_O}{[O_2]_O} = \frac{V_O(D_{32})}{V_O(\widetilde{D}_{32})} = \frac{D_{32}}{\widetilde{D}_{32}} = K_{32} \quad \text{eq.S14}$$

where $[O_2]_W$ and $[O_2]_O$ indicate the concentrations of O_2 in the water and oil phases, respectively; V_W and V_O are the volume of water and oil phases.

Kinetic rate and kinetic constants

From **Table 1**, the reactions for LOO* with LH or with BODIPY 665/676 over time can be described as,

$$\text{[R.3] LOO* + LH} \xrightarrow{k_3} \text{LOOH + L*}$$

$$\text{[R.9] LOO* + BODIPY} \xrightarrow{k_{BODIPY}} \text{non-radical products}$$

where k_{BODIPY} and k_3 are kinetic constants. The kinetic rates for LOO* to react with LH or BODIPY 665/676 over time corresponding to R.3 and R.9 can be expressed as r^{R3}_{LOO*} and r^{R9}_{LOO*}, respectively,

$$r^{R3}_{LOO*} = k_3 \times [LOO*][LH]$$

$$r^{R9}_{LOO*} = k_{BODIPY} \times [LOO*][BODIPY]$$

Although k_{BODIPY} is two times higher than k_3 (**Table S2**), the kinetic model showed that the kinetic rate r^{R9}_{LOO*} is 4.5×10^7 times lower than r^{R3}_{LOO*} due to the high initial concentration of LH compared to the initial concentration of BODIPY.

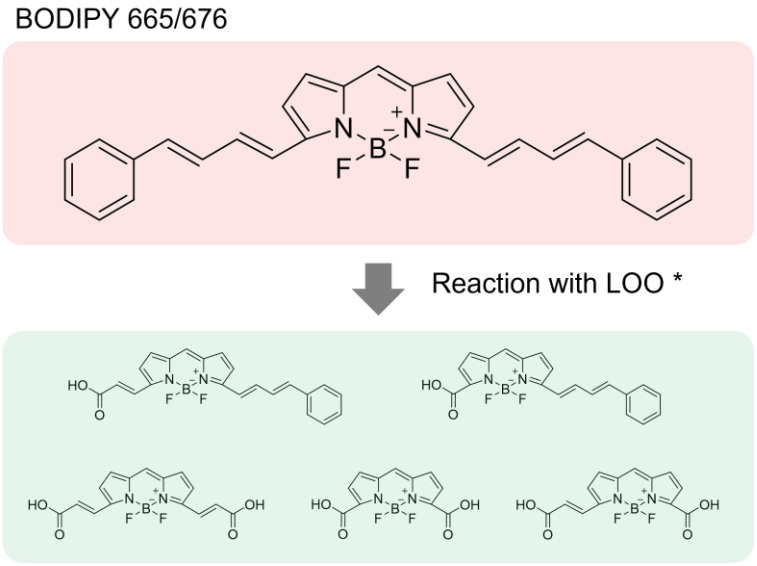

Figure S4. The non-oxidized structure and possible modified structures of BODIPY 665/676 upon oxidation

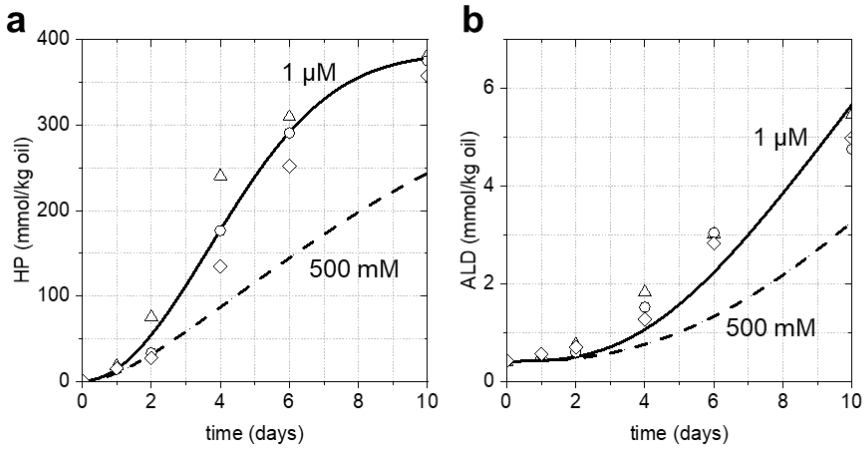

Figure S5. The formation of lipid oxidation products at various concentrations of BODIPY 665/676. Comparison between the simulations of hydroperoxides (**a**) and aldehydes (**b**) concentrations over time with 0, 1, and 50 µM (all three in overlapping solid black lines) and with 500 mM (dashed lines) of BODIPY 665/676.

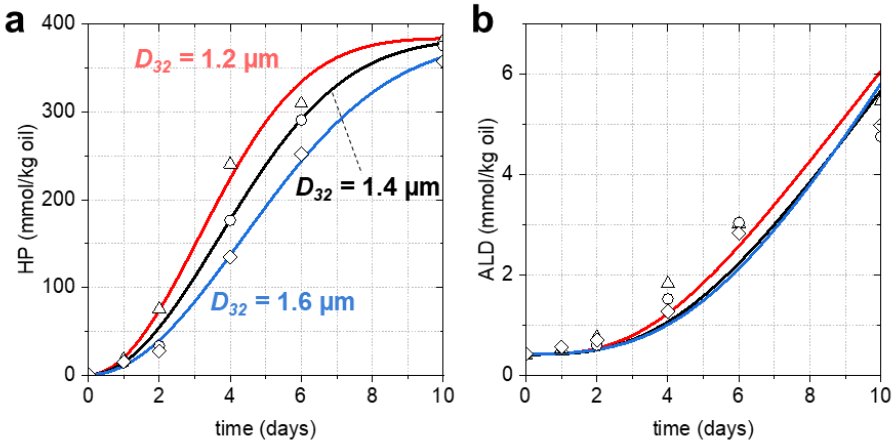

Figure S6. Effect of the droplet sizes (D_{32}) with the deviations (± 0.2 µm) on the formation of hydroperoxides (**a**) and aldehydes (**b**) over incubation in colloid mill-made emulsions stabilized by 2 wt% WPI. The concentration of BODIPY 665/676 was fixed at 1 µM, and only droplet sizes (D_{32}) were varied. Red, black, and blue solid lines show the simulation results from different droplet sizes, respectively, for 1.2, 1.4, and 1.6 µm. The experimental data set (from **Figure 2**) is included for the comparison. We attribute the difference in the formation of lipid oxidation products between 0, 1, and 50 µM BODIPY 665/676 emulsions to the small droplet size difference from the separate emulsification steps.

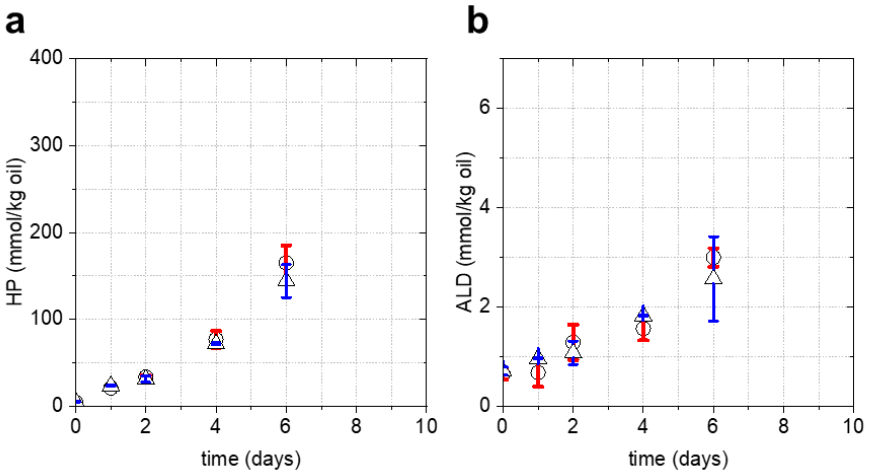

Figure S7. Validation of using BODIPY 665/676 to probe oxidation by experiments. (a-b) The formation of hydroperoxides (HP) (a) and aldehydes (ALD) (b) in the absence and presence of BODIPY 665/676 as measured by NMR. The samples were prepared with a colloid mill (polydisperse emulsions) and stabilized by 2 wt.% WPI. Markers corresponding to samples containing 0 (triangle) and 1 (circles) μM of BODIPY 665/676. Error bars (sometimes hidden by the symbol) denote standard deviations of four measurements including two independent sample preparations.

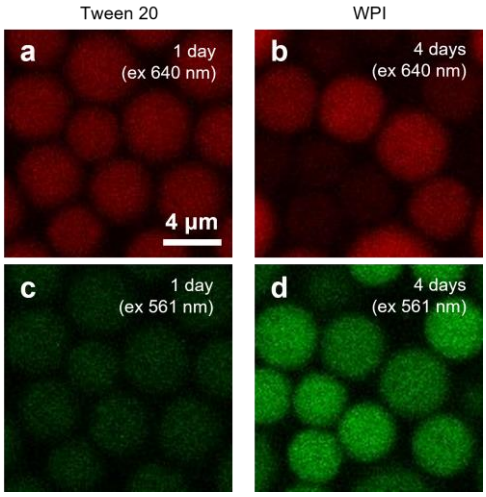

Figure S8. Combined channel images of non-oxidized (ex 640 nm) and oxidized (ex 561 nm) BODIPY 665/676 in Tween 20- and WPI-stabilized emulsions. Tween 20-stabilized emulsions showed the decrease of BODIPY 665/676 excited at 640 nm, whereas they did not show an increase in channel representing oxidized BODIPY excited at 561 nm. In contrast, both the decrease in native fluorescence and the increase in oxidized BODIPY 665/676 were observed in WPI-stabilized emulsions.

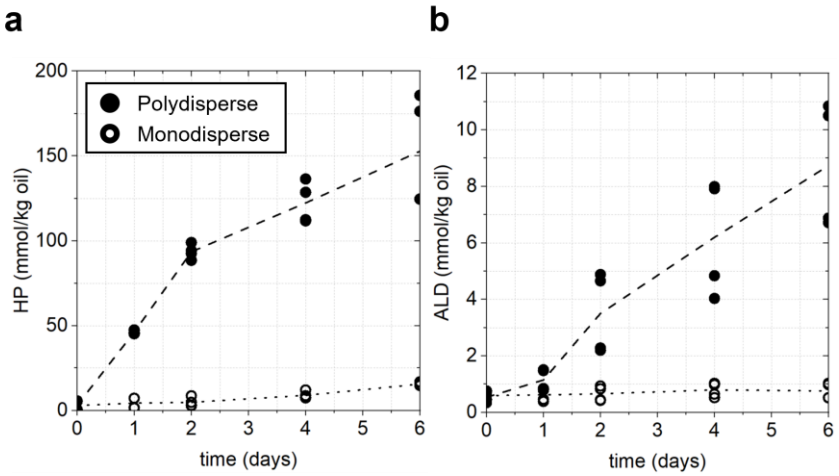

Figure S9. Lipid oxidation in Tween 20-stabilized emulsions. The formation of hydroperoxides (**a**) and aldehydes (**b**) in the colloid mill-made polydisperse emulsions stabilized by Tween 20 proceeded faster than in monodisperse emulsions made with microfluidic devices. The difference in droplet sizes caused this faster oxidation in polydisperse emulsions, as we described in **Figure 1**.

References

(1) Takahashi, A.; Takahashi, R.; Hiromori, K.; Shibasaki-Kitakawa, N. Quantitative Evaluation of Oxidative Stability of Biomembrane Lipids in the Presence of Vitamin E. *J Am Oil Chem Soc* **2021**, *98* (5), 567–579. https://doi.org/10.1002/AOCS.12480.

(2) Rojas Wahl, R. U.; Zeng, L.; Madison, S. A.; DePinto, R. L.; Shay, B. J. Mechanistic Studies on the Decomposition of Water Soluble Azo-Radical-Initiators. *Journal of the Chemical Society, Perkin Transactions 2* **1998**, No. 9, 2009–2018. https://doi.org/10.1039/A801624K.

(3) Niki, E. Role of Vitamin e as a Lipid-Soluble Peroxyl Radical Scavenger: In Vitro and in Vivo Evidence. *Free Radic Biol Med* **2014**, *66*, 3–12. https://doi.org/10.1016/J.FREERADBIOMED.2013.03.022.

(4) Napolitano, G.; Fasciolo, G.; Meo, S. Di; Venditti, P. Vitamin E Supplementation and Mitochondria in Experimental and Functional Hyperthyroidism: A Mini-Review. **2019**. https://doi.org/10.3390/nu11122900.

(5) Decker, E. A.; Hultin, H. O. Lipid Oxidation in Muscle Foods via Redox Iron. **1992**, 33–54. https://doi.org/10.1021/BK-1992-0500.CH003.

(6) Yoshida, Y.; Shimakawa, S.; Itoh, N.; Niki, E. Action of DCFH and BODIPY as a Probe for Radical Oxidation in Hydrophilic and Lipophilic Domain. *Free Radic Res* **2003**, *37* (8), 861–872. https://doi.org/10.1080/1071576031000148736.

(7) Babbs, C. F.; Steiner, M. G. Simulation of Free Radical Reactions in Biology and Medicine: A New Two-Compartment Kinetic Model of Intracellular Lipid Peroxidation. *Free Radic Biol Med* **1990**, *8* (5), 471–485. https://doi.org/10.1016/0891-5849(90)90060-V.